AGU PUBLICATIONS

Geophysical Research Letters

RESEARCH LETTER
10.1002/2014GL060764

Key Points:
- Robust decline in blocks and waviness as meridional temperature gradient reduces
- A dynamical link between Arctic warming and weather extremes needs further study
- Blocks occur in the absence of topography or zonally asymmetric forcings

Supporting Information:
- Readme
- Figures S1–S3

Correspondence to:
P. Hassanzadeh,
hassanzadeh@fas.harvard.edu

Citation:
Hassanzadeh, P., Z. Kuang, and B. F. Farrell (2014), Responses of midlatitude blocks and wave amplitude to changes in the meridional temperature gradient in an idealized dry GCM, *Geophys. Res. Lett.*, *41*, 5223–5232, doi:10.1002/2014GL060764.

Received 5 JUN 2014
Accepted 4 JUL 2014
Accepted article online 10 JUL 2014
Published online 23 JUL 2014

Responses of midlatitude blocks and wave amplitude to changes in the meridional temperature gradient in an idealized dry GCM

Pedram Hassanzadeh[1], Zhiming Kuang[2], and Brian F. Farrell[2]

[1]Center for the Environment and Department of Earth and Planetary Sciences, Harvard University, Cambridge, Massachusetts, USA, [2]Department of Earth and Planetary Sciences and School of Engineering and Applied Sciences, Harvard University, Cambridge, Massachusetts, USA

Abstract The response of atmospheric blocks and the wave amplitude of midlatitude jets to changes in the midlatitude to pole, near-surface temperature difference (ΔT), is studied using an idealized dry general circulation model (GCM) with Held-Suarez forcing. Decreasing ΔT results in slower zonal winds, a mean state with reduced meridional gradient of the 500 hPa geopotential height ($Z500$), a smaller variance of $Z500$ anomalies, and a robust decrease in blocks and meridional amplitude of waves. Neglecting the decrease of variance associated with reduced ΔT would lead to the incorrect expectation that mean states with smaller $Z500$ gradients produce more blocks and higher wave amplitudes. Our results suggest further investigation of the hypothesis that reduced ΔT due to Arctic Amplification would increase blocking events and wave amplitude, hence leading to more midlatitude extreme weather events.

1. Introduction

A question of significant scientific and societal importance is whether the recent increase in certain types of weather extremes is related to global climate change [*Coumou and Rahmstorf*, 2012; *Hoerling et al.*, 2013]. One of the prominent components of climate change is Arctic Amplification (AA), i.e., the faster warming of high latitudes compared to the rest of the Northern Hemisphere [*Screen and Simmonds*, 2010; *Intergovernmental Panel on Climate Change*, 2007]. AA results in a smaller midlatitude to pole, near-surface temperature difference, referred to as ΔT hereafter [*Walsh*, 2014, Figure 8]. *Francis and Vavrus* [2012] and *Liu et al.* [2012] (FVL12) have recently suggested that reduced ΔT changes the midlatitude atmospheric circulation by slowing down the zonal winds and increasing the north-south meandering (i.e., wave amplitude and waviness) of the jet stream, resulting in slower progression of weather systems and more frequent atmospheric blocking events. Slowly moving weather systems and blocks cause persistent weather patterns and can lead to weather extremes such as heat waves [*Dole et al.*, 2011; *Black et al.*, 2004], cold spells [*Trigo et al.*, 2004; *Buehler et al.*, 2011], drought [*Green*, 1977], and heavy precipitation [*Park et al.*, 2011; *Hong et al.*, 2011 (see also *Screen and Simmonds* [2014]).

While recent weather extremes, in particular, the severe 2014 winter in North America, have raised the public interest in the FVL12 hypothesis, the scientific community is still examining the theoretical and observational evidence for this hypothesis [*Wallace et al.*, 2014; *Vihma*, 2014; *Walsh*, 2014]. Recent studies by *Tang et al.* [2013a, 2013b] have provided further observational support for a link between changes in the cryosphere and hot summer/cold winter extremes in the northern midlatitudes in the past 30 years. However, Barnes and her colleagues used several reanalyses of the same time period and did not find a significant increase in wave amplitude [*Barnes*, 2013] or a clear hemispheric increase in blocking [*Barnes et al.*, 2014]. Furthermore, focusing on European winters, *Woollings et al.* [2014] used the four Coupled Model Intercomparison Project Phase 5 (CMIP5) models with the best blocking climatology and found no conclusive evidence for a link between changes in the Arctic and Eurasian or Greenland blocks. These later studies conclude that even if AA favors wavier jet streams and more blocks in the midlatitudes, the influence is weak compared to natural variability [see also *Screen et al.*, 2013; *Rinke et al.*, 2013; *Peings and Magnusdottir*, 2014; *Screen*, 2014; *Screen and Simmonds*, 2014; *Cheung et al.*, 2013; *Vihma*, 2014; *Liu et al.*, 2014].

The disagreement among these studies might be due to the sensitivity of results to the methodology used to analyze waviness [*Barnes*, 2013; *Screen and Simmonds*, 2013] and temperature correlations

[*Woollings et al.*, 2014], indices and reanalyses used in studying blocking trends [*Barnes et al.*, 2014], poor performance of CMIP5 (and older) models in simulating blocks [*Anstey et al.*, 2013; *Dunn-Sigouin and Son*, 2013; *D'Andrea et al.*, 1998], and lack of long enough observations/simulations. Furthermore, the effect of AA on blocks and waviness in reanalyses and full GCMs is entangled with the influence of additional factors such as internally generated ocean-atmosphere variability and other changes in the thermal mean state (section 3.1). These issues complicate investigation of the FVL12 mechanism and suggest adopting an approach using a hierarchy of models from highly simplified to comprehensive GCMs (in which various of these confounding mechanisms can be circumvented) along with observation.

In this letter we study a primary aspect of the theoretical basis for the hypothesis of FVL12 by focusing on the following question: how do midlatitude blocks and wave amplitude change with ΔT? To answer this question, we use an idealized model, a dry dynamical core with the forcing of *Held and Suarez* [1994]. The simplicity of this model enables us to isolate the role of ΔT and perform long high-resolution simulations, from which we can obtain robust statistics for the responses of waviness and blocking to ΔT. The response of the model's mean state to changes in ΔT is reasonably consistent with observation (section 3.1), the model retains the physics essential for the mechanism proposed by FVL12, and while some of the physical processes excluded from this model and other simplifications applied in our idealized setup (section 2.1) might have an impact on the response of blocks and wave amplitude to ΔT, the FVL12 mechanism is not related to such effects. This idealized model provides a simplified dynamical framework for investigating the FVL12 mechanism and complements the ongoing efforts with observation and a hierarchy of GCMs.

2. Methods

2.1. Simulations

We use the Geophysical Fluid Dynamics Laboratory dry dynamical core forced by Newtonian relaxation of temperature to a prescribed zonally symmetric radiative equilibrium state with a specified equator-to-pole, *surface* temperature difference ΔT_y as described in *Held and Suarez* [1994] (note the distinction between ΔT_y, a forcing parameter, and ΔT, a property of the mean state; see section 3.1). The model does not have seasonal or diurnal cycles, topography, a cryosphere or hydrosphere, and hence the related physical parameterizations needed in full GCMs. Despite such simplifications, the dry core produces reasonable mean and low-frequency properties of the atmospheric circulation [*Held and Suarez*, 1994; *Gerber et al.*, 2008] and has been used to study various aspects of large-scale dynamics [e.g., *Polvani and Kushner*, 2002; *Walker and Schneider*, 2006; *Butler et al.*, 2010; *Kidston and Vallis*, 2010].

Although quasi-stationary planetary waves forced by topography or other zonally asymmetric features are sometimes suggested to be essential for blocking formation [*Hu et al.*, 2008], blocks have been found to occur frequently in the absence of such zonally varying forces in aquaplanet [*Hu et al.*, 2008] and dry core [*Kunz et al.*, 2009] simulations [see also *Nakamura et al.*, 1997]. As shown later, strong long-lived blocks are common in our simulations, which are free of forced quasi-stationary planetary waves.

The model is run with horizontal resolution T85 ($\sim 1.4° \times 1.4°$) and 30 evenly spaced sigma levels (T85L30). Each run is integrated for 29,500 days with 10 min time steps, and the first 400 days are not analyzed to allow enough time for spin-up (*run* and *case* hereafter refer to an individual simulation and simulations with the same ΔT_y, respectively). Five cases with $\Delta T_y = 40, 50, 60, 70, 80$ K are studied, while all other physical parameters are the same as *Held and Suarez* [1994] (which has $\Delta T_y = 60$ K). In section 3.1 we compare the response of the model's mean state to ΔT_y with the trends observed in full GCMs and reanalysis. For each case, three simulations with slightly different small initial perturbations are run to produce a three-member ensemble. Daily averaged data are obtained from 6 h outputs for each run and interpolated into a $2.8° \times 2.8°$ grid for analysis. Because the forcing is hemispherically symmetric, both hemispheres are included in the analysis. We repeated the analysis for runs with lower resolution T63L25 and found no change in the trends reported in section 3.

2.2. Blocking Index

There is no consensus on the definition of blocks, but the term usually refers to quasi-stationary synoptic-scale anticyclones that last for days or even weeks, hence blocking or diverting the eastward progress of weather systems [e.g., *Rex*, 1950; *Dole and Gordon*, 1983; *Pelly and Hoskins*, 2003; *Barriopedro et al.*, 2010]. On the equatorward side of the anticyclone, the westerlies are weakened and even reversed, and the anticyclones might be accompanied by a cyclone in a dipole (Rex block) or by two cyclones in a

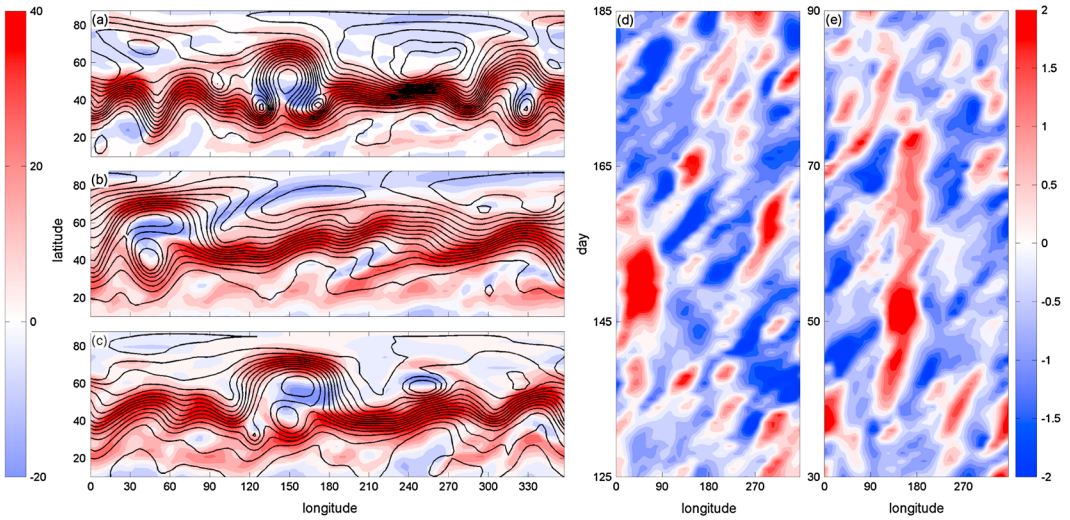

Figure 1. Examples of blocks in simulations with $\Delta T_y = 60$ K. $Z500$ (contour) and 300 hPa zonal wind (shading, m/s) for the following: (a) an Ω block around longitude 150° on day 249, (b) a Rex block splitting the jet around longitude 50° on day 147, and (c) a large block significantly displacing the jet poleward around longitude 150° on day 51. In all examples, easterlies with magnitude of around −20 m/s replace the mean state westerlies south of the anticyclonic anomalies (see Figure S1 for anomalies). Zonally averaged time mean 300 hPa zonal winds around 45° and 55°N are about +28 and +15 m/s, respectively. (d, e) The Hovmöller diagrams of the blocks in Figures 1b and 1c, respectively. The shading shows $Z500$ anomalies, averaged over 57°–63°N and normalized by σ_{max} (see text). Both blocks are clearly persistent and stationary.

Ω-shaped (Ω block) structure (Figure 1 and Figure S1 in the supporting information). Lack of a universally accepted definition and a complete theory for the generation, longevity, and decay of blocks [e.g., *Tyrlis and Hoskins*, 2008] have complicated the development and evaluation of blocking indices [*Barriopedro et al.*, 2010; *Barnes et al.*, 2011]. Here we use an index similar to the hybrid index of *Dunn-Sigouin and Son* [2013] with several modifications. As the main goal of this work is to compare blocks among different cases, we have tried to avoid any assumption or parameter that might bias the index toward any mean state.

The index uses the daily 500 hPa geopotential height ($Z500$) to identify blocks. Briefly, the $Z500$ anomalies (with respect to zonally averaged time mean $Z500$, noted as $\bar{Z}500$ hereafter and shown in Figure 2a) are calculated at every longitude ϕ, latitude θ, and day n.

1. Anomalies are normalized by the maximum of the zonally averaged standard deviation of $Z500$ (σ_{max}) of each run; σ_{max} is practically the same in each case but can vary significantly with ΔT_y, e.g., σ_{max} is around 134 m and 197 m for cases with $\Delta T_y = 40$ and 80 K, respectively (Figure 2b). By inspection, we have found that normalization using the σ_{max} of each case, rather than the same value for all cases, provides a better measure of the strength of an anomaly to influence and obstruct the zonal flow. As discussed in section 3.2, using the same normalization for all cases does not alter the conclusions of this work. Also note that following *Sausen et al.* [1995] and *Barriopedro et al.* [2010], and unlike *Dole and Gordon* [1983, equation (1)] and *Dunn-Sigouin and Son* [2013], we do not scale the anomalies with the Coriolis parameter. We have found that when the mean states are different, this scaling produces a bias favoring cases with equatorward shifted blocks and may result in missing some of the anomalies that truly affect the zonal flow.
2. Anomalies that are larger than or equal to a threshold α are stored in $B(\phi, \theta, n)$. Here we use $\alpha = 1.5$ or 2. Subsequently, for every grid point in B (e.g., $B(\phi_o, \theta_o, n_o)$), we check if at least six out of the eight adjacent grid points (i.e., at $\phi_o \pm \Delta\phi$ and $\theta_o \pm \Delta\theta$) are also in $B(\theta, \phi, n_o)$ (as a reminder, $\Delta\phi$ and $\Delta\theta$ are $\sim 2.8°$). If this requirement for spatial extent is satisfied, that grid point is stored in $S(\theta_o, \phi_o, n_o)$. The results are not sensitive to the choice of six.
3. If grid point (ϕ_o, θ_o) is *not* in S at day n_o, but is in S consecutively from day $n_o + 1$ to at least day $n_o + D$, it is stored in $E(\theta_o, \phi_o, n_o + 1)$. We have used $D = 7$ or 14 days.
4. Finally, we require reversal of $Z500$ in at least 1 day out of the D days. On each day, we average $Z500$ over $(\phi_o \pm 2\Delta\phi, \theta_o \pm \Delta\theta)$ and check if it is larger than or equal to any $Z500$ averaged over $(\phi_o \pm 2\Delta\phi, \theta_c \pm \Delta\theta)$,

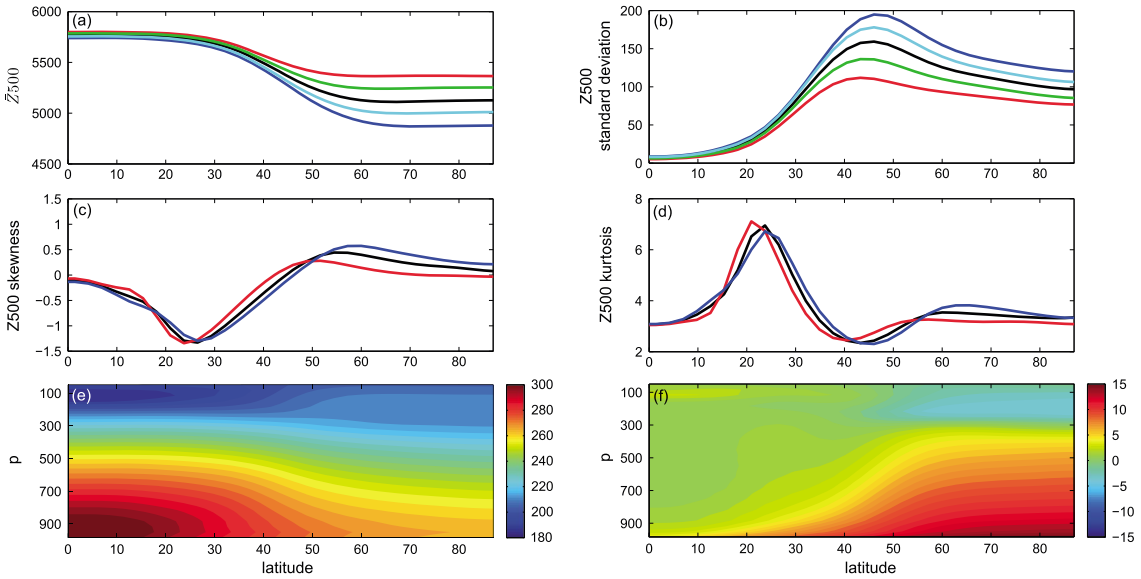

Figure 2. Zonally averaged statistical measures of $Z500$ for runs with $\Delta T_y = 40$ (red), 50 (green), 60 (black), 70 (cyan), and 80 K (blue). (a) $\bar{Z}500$ (m): time mean; (b) σ (m): standard deviation; the maximum standard deviation σ_{max} for $\Delta T_y = 60$ K is $\sim$ 160 m, agreeing with the observed value in the spring and fall of Northern Hemisphere [e.g., *Shukla and Mo*, 1983, Figure 1]. (c) Skewness. (d) Kurtosis. Only three cases are shown in Figures 2c and 2d for clarity. (e) Zonally averaged time mean temperature (K) for the case with $\Delta T_y = 60$ (K). (f) Response of zonally averaged time mean temperature (K) to reducing ΔT_y from 60 to 40 (K), showing warming in near-surface high latitudes as ΔT_y decreases.

where θ_c is 3 to 5 grid points equatorward of θ_o. We average over a larger longitudinal extent to better handle Ω blocks. We demand reversal only for 1 day because blocks may not necessarily reverse $Z500$ throughout their evolution. Nevertheless, relaxing the reversal requirement barely changes the blocking statistics (and has no effect on the reported trends) as the relatively strong blocks considered here (with $\alpha = 1.5$ or 2) often reverse the zonal wind.

5. A grid point (ϕ_o, θ_o) which is in E on day n_o and satisfies the reversal requirement is marked blocked from day n_o to $n_o + D - 1$.

Rather than reporting the number (or frequency) of blocking events or blocked grid points, here we present blocked-area-per-day at each latitude, calculated by summing the area of all blocked grid points in both hemispheres over all longitudes and days and then dividing by the length of each run, 29,100 days (note that the area associated with a 2.8° × 2.8° grid point at latitude θ is $\sim 9.7 \times 10^4 \mid \cos(\theta) \mid$ km^2). By reporting area, the spatial extent of blocking events is included in the statistics. Furthermore, the change in area of a grid point with latitude is taken into account, which is particularly important to avoid biases in the blocking index because the latitudinal distribution of blocks varies with ΔT_y (section 3.2). As discussed later, ignoring the area change with latitude does not affect the conclusions of this work.

2.3. Wave Amplitude Analysis

Barnes [2013] and *Screen and Simmonds* [2013] have recently pointed out the sensitivity of wave amplitude analyses to the selected $Z500$ isopleths and to "how waves are conceptualized." To minimize potential biases given the substantial changes in the mean state with ΔT_y, here we choose different sets of $Z500$ isopleths for different cases based on their mean states. Each set includes six isopleths: Z_1 is $\bar{Z}500$ at the latitude of the maximum zonally averaged time mean 500 hPa zonal wind; Z_4 is $\bar{Z}500$ at the latitude of σ_{max}; $Z_2 = Z_4 + \sigma_{max}/2$; $Z_3 = Z_4 + \sigma_{max}/4$; $Z_5 = Z_4 - \sigma_{max}/4$; and $Z_6 = Z_4 - \sigma_{max}/2$ (see Figure 4b for the values). For a selected isopleth Z_j, in each hemisphere, the latitude $y_j(\phi, n)$ is calculated for all longitudes and days. Fourier analysis is used to decompose y_j into $a_{m,j}(n) \exp(im\phi)$ terms at each day, and the Fourier coefficients $a_{m,j}(n)$ of wave numbers 1–15 are used to calculate the daily meridional wave amplitude $A_j(n)$ using the Parseval's theorem (see supporting information for details). Using wave numbers 1–5 or 1–10 to calculate $A_j(n)$ does not affect the trends reported in section 3.3. Figure S2 shows examples of low- and high-amplitude waves for different cases.

3. Results

3.1. Changes in Mean State

The idealized model's mean state changes in response to changing ΔT_y [e.g., *Gerber and Vallis*, 2007; *Kidston and Vallis*, 2010]. Here we briefly compare the response with trends that are seen in full GCMs and reanalysis. As shown in Figures 2e and 2f and S3a–S3c, although the equator-to-pole, surface temperature difference ΔT_y is varied in the radiative forcing, the mean state temperature primarily changes in the midlatitude to pole lower troposphere, most strongly near the surface at high latitudes. Therefore, changing ΔT_y mainly changes the midlatitude to pole, near-surface temperature difference ΔT, which is suitable for the purpose of this study. The ΔT trends show a clear effect of AA in CMIP5 simulations with increased carbon dioxide and in reanalysis [*Walsh*, 2014]. The structure of ΔT is similar in the idealized model and reanalysis/CMIP5 results, although more confined both vertically and meridionally to the polar surface in the latter (where it also varies zonally and seasonally). Nonetheless, we again emphasize the purpose of an idealized approach and its advantages. For example, isolating the role of ΔT is not easy if full GCMs or reanalyses are used, as the confounding presence of other thermal forcings, various physical processes, and feedbacks complicate the analysis, e.g., warming in the tropical upper troposphere in the CMIP5 simulations [*Lu et al.*, 2008, Figure 2b] increases the upper tropospheric meridional temperature difference and obscures the impact of ΔT alone on the blocks and waviness.

With decrease of ΔT, the 500 hPa height rises in the high latitudes [*Francis and Vavrus*, 2012; *Walsh*, 2014], reducing the midlatitude meridional gradient of $\bar{Z}500$ ($\Delta\bar{Z}500$ hereafter). This is also the response of $\bar{Z}500$ in the idealized model (Figure 2a). Figures S2d–S2f show that the midlatitude zonal winds weaken as ΔT reduces, consistent with thermal wind balance and reanalysis [*Walsh*, 2014, Figure 10]. We note that the speed of the midlatitude westerlies increases in CMIP5 simulations of a warmed climate [*Lu et al.*, 2008; *Barnes and Polvani*, 2013], perhaps due to other effects mentioned above. We also point out that the structures of the mean state zonal winds in the idealized model (Figure S3e) and CMIP5 [*Lu et al.*, 2008, Figure 2d] are similar.

Reanalysis [*Archer and Caldeira*, 2008] and CMIP5 simulations with increased carbon dioxide [*Lu et al.*, 2008; *Barnes and Polvani*, 2013] show a poleward shift of the midlatitude jets, but the underlying physics is not well understood [e.g., *Riviére*, 2011; *Lu et al.*, 2010; *Kidston and Vallis*, 2012]. Therefore, it is unclear from these results how the jet latitude changes with ΔT alone, because of the presence of various other processes and thermal forcings (such as tropical upper tropospheric heating and stratospheric cooling). Figures S3d–S3l show equatorward shifts of the jet and eddy fluxes with reducing ΔT, consistent with findings in other studies with simplified models [*Butler et al.*, 2010; *Lu et al.*, 2010].

The behavior of the primary components of the FVL12 mechanism (i.e., ΔT, $\Delta\bar{Z}500$, and zonal winds) in the idealized model is reasonably consistent with observation and full GCMs. Therefore, this idealized model qualifies as a member of a hierarchy of simplified to comprehensive GCMs needed to study this mechanism.

3.2. Changes in Blocks

Figures 3a–3c present blocked-area-per-day as a function of latitude for blocks identified with three sets of (α, D). Figure 3d shows the total blocked-area-per-day over latitudes 30°–70° for the results in Figures 3a–3c. The response of blocks to reducing ΔT_y exhibits two robust features: (1) an equatorward shift of the blocking distribution and (2) a decrease in blocked area.

The first feature is consistent with the equatorward shift of the zonal winds and eddy fluxes with decreasing ΔT_y. The second robust feature answers the first part of the question asked in section 1: reducing ΔT_y leads to a smaller blocked-area-per-day. The difference is more pronounced for larger (α, D). Comparing the ensemble mean of cases with $\Delta T_y = 40$ and 80 K, the total blocked-area-per-day between 30° and 70° increases by a factor of 1.3, 3.4, and 4.2 for $(\alpha, D) = (1.5, 7), (2, 7)$, and $(1.5, 14)$, respectively (Figure 3d). For $(2, 14)$ (not shown), blocks are rarely found: no blocked point is identified in any $\Delta T_y = 40$ K run, while the $\Delta T_y = 80$ K has an ensemble mean of 650 km^2/day. Note that the trends reported here are not sensitive to our choices to normalize the $Z500$ anomalies with different σ_{max} or to use blocked area instead of blocked grid point. In fact, cases with greater ΔT_y have larger σ_{max} and blocks shifted toward higher latitudes (where area per grid point is smaller); therefore, both choices favor cases with smaller ΔT_y. Furthermore, reporting area has greatly reduced the contribution of "high-latitude blocks" to the statistics. High-latitude blocks do not obstruct the jet but rather displace it equatorward [*Berrisford et al.*, 2007; *Woollings et al.*, 2008], and their identification as blocks is regarded as a weakness in indices that search all latitudes [*Barnes et al.*, 2011].

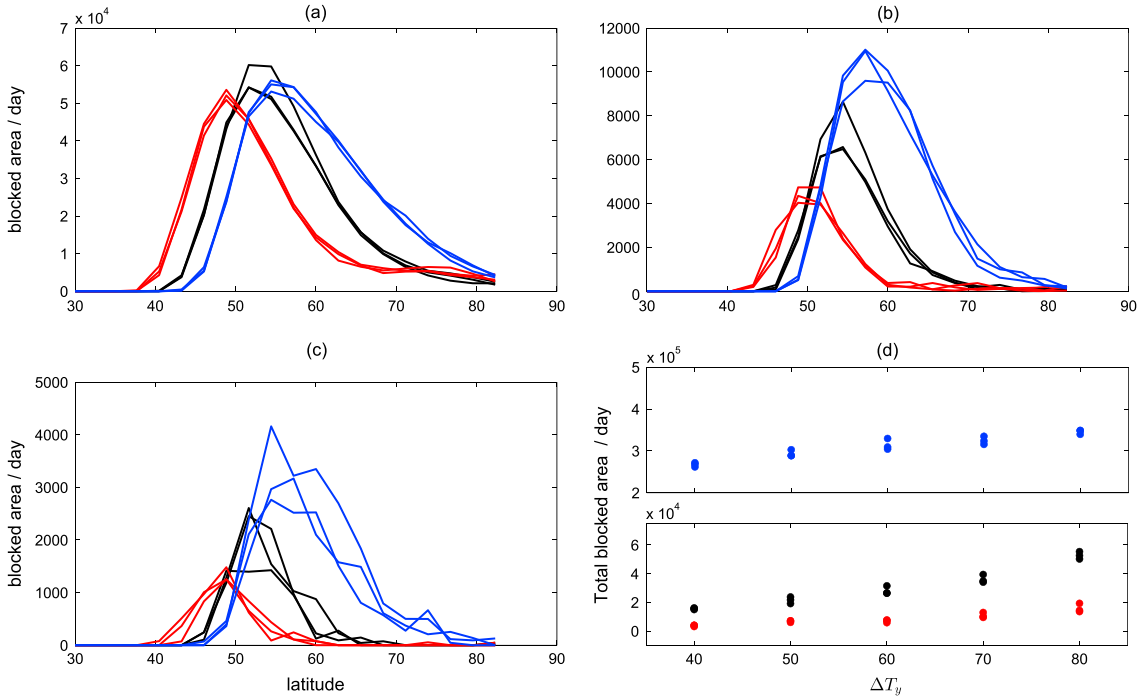

Figure 3. (a–c) Latitudinal distribution of blocked-area-per-day (km^2/day per 2.8° latitude bin) for $\Delta T_y = 40$ (red), 60 (black), and 80 K (blue): (a) $\alpha = 1.5, D = 7$, (b) $\alpha = 1.5, D = 14$, and (c) $\alpha = 2, D = 7$. The three runs of each case are shown separately, and their difference is an indicator of statistical uncertainties. (d) Total blocked-area-per-day (km^2/day) summed over latitudes 30°–70° versus ΔT_y. (top) Blocks with $\alpha = 1.5, D = 7$ (blue circles); (bottom) blocks with $\alpha = 2, D = 7$ (black circles) and $\alpha = 1.5, D = 14$ (red circles). All three positive trends are significant with $p < 10^{-5}$ from a two-tailed t test.

The lack of a complete understanding of blocking dynamics and the existence of a variety of theories [*Tyrlis and Hoskins*, 2008] obscure attempts to isolate and identify, with certainty, the mechanism(s) directly responsible for the observed changes of blocking statistics with ΔT_y. We leave investigation of these mechanisms to future work; however, below we present a brief discussion to clarify the influence of $\Delta\bar{Z}500$ and the latitude and speed of the midlatitude jet.

A mean state with a smaller $\Delta\bar{Z}500$ might be expected to favor blocks more than a mean state with a larger gradient, because a reversal (of $Z500$ gradient) might seem easier to achieve in the former. However, our results show the opposite: more blocks occur in cases with greater ΔT_y, which have larger $\Delta\bar{Z}500$ (Figure 2a). What is missing in the above line of reasoning is the fact that the strength of the $Z500$ anomalies also changes with the mean state. As shown in Figure 2b, cases with greater $\Delta\bar{Z}500$ also have larger standard deviation of $Z500$ (σ), consistent with the increase of baroclinicity with ΔT_y [see also *Screen*, 2014]. In fact, changes in $\Delta\bar{Z}500$ and σ are nearly proportional: for cases with $\Delta T_y = 40, 60, 80$ K, we find $\Delta\bar{Z}500 \sim -16.6, -22.6, -27.6$ m/degree and $\sigma \sim 97, 140, 167$ m (i.e., $\sigma/\Delta\bar{Z}500 \sim -0.171, -0.161, -0.165$ degree), respectively (where $\Delta\bar{Z}500$ and σ are approximated and averaged in the ranges that $Z500$ varies almost linearly for each case.) Therefore, to the first order, all cases have the same capability to locally reduce or even reverse the meridional gradient of $Z500$ and produce blocks. This is because, assuming a Gaussian $Z500$ distribution, the probability that the anomalies with meridional extent A have a meridional gradient larger than $\Delta\bar{Z}500$ is $\mathrm{erfc}(\frac{A\Delta\bar{Z}500}{\sigma\sqrt{2}})$ (where erfc is the complementary error function). Therefore, because our results show a robust increase in blocks with $\Delta\bar{Z}500$, deviations from Gaussianity in the $Z500$ distribution (see Figures 2c and 2d for skewness and kurtosis), changes in the distribution of persistent $Z500$ anomalies, and the role of other processes must be investigated to explain the difference in blocking statistics.

It is not clear how the latitude or speed of the midlatitude jets influences blocks; therefore, one should remain cautious at this time in ascribing causality to individual mechanisms. For example, the negative phase of the North Atlantic Oscillation (NAO$^-$), characterized by an equatorward shifted eddy-driven Atlantic jet, is correlated with increased blocks over North Atlantic [*Barriopedro et al.*, 2006], which might suggest that an equatorward shifted jet inherently favors more blocks. However, this effect of NAO$^-$ on blocks has been attributed to modulation of surface air temperature distribution to a state favoring more

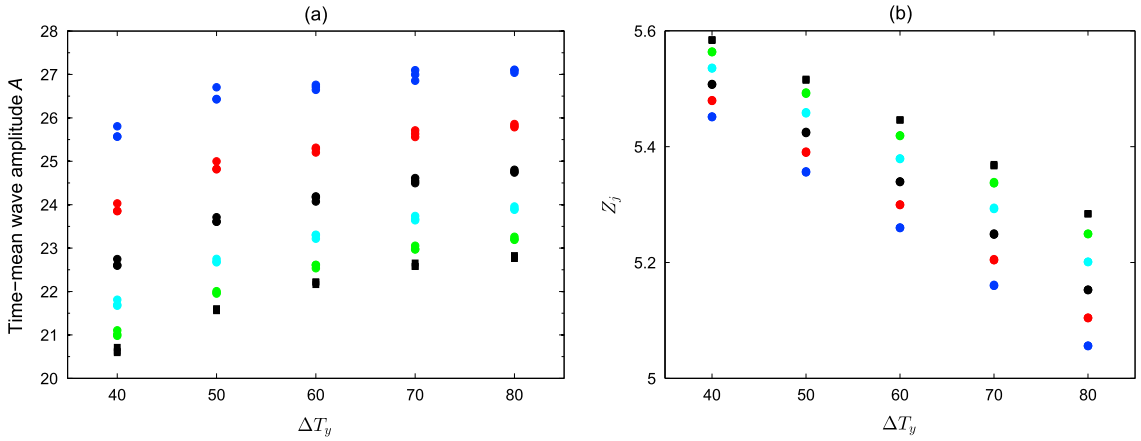

Figure 4. (a) Time mean wave amplitude A (degree) obtained from wave numbers 1–15 versus ΔT_y for Z_1 (black squares), Z_2 (green circles), Z_3 (cyan circles), Z_4 (black circles), Z_5 (red circles), and Z_6 (blue circles). (b) Values of Z_j (km) in each case. The three runs of each case are shown separately, and their difference is an indicator of statistical uncertainties. All positive trends in Figure 4a are significant with $p < 10^{-5}$ from a two-tailed t test. Calculations using wave numbers 1–5 or 1–10 yield similar significant positive trends.

blocks [*Shabbar et al.*, 2001]. Alternatively, it has been recently proposed that NAO$^-$ is actually caused by more frequent high-latitude blocks over Greenland, displacing the jet equatorward [*Woollings et al.*, 2008]. Therefore, the NAO-related changes in blocking statistics do not provide a compelling case for a specific dynamical link between the jet latitude and blocks.

A decrease in blocking events with a poleward shift of the jet has been observed in CMIP3/CMIP5 simulations under global warming scenarios [e.g., *Barnes and Hartmann*, 2010; *Barnes et al.*, 2013]. However, these models underestimate the present-day blocking frequency (obtained from reanalysis), even though the models have the jet equatorward of the jet position in reanalysis [*Barnes and Hartmann*, 2010], suggesting that the relationship is not simple and that other processes play a role. Similarly, the relation between the speed of the zonal wind and frequency of blocks can be misleading. Observing a local correlation between high blocking frequency and weak westerlies does not necessarily mean that a slower jet favors more blocks. This is because blocking indices, particularly the ones that require zonal wind reversal, can be thought as an inverse measure of the strength of the local westerlies, and the observed weak westerlies might be just a consequence of more frequent blocks [see, e.g., *Tyrlis and Hoskins*, 2008, section 3].

3.3. Changes in Wave Amplitude

Figure 4a shows the time mean wave amplitude A as a function of ΔT_y for the six isopleths described in section 2.3. Figure 4b presents the value of Z_j for each case, which are noticeably different as a result of changes in the jet latitude, latitude, and magnitude of σ_{max}, and the $\bar{Z}500$ profile. However, these isopleths are chosen based on the dynamics of the mean state. Results of Figure 4 show a small, but robust, increase in the wave amplitude with ΔT_y, which answers the second part of the question asked in section 1.

One might expect that reducing ΔT_y leads to larger wave amplitudes, because with the *same* $Z500$ anomaly, a larger meridional extension of an isopleth is achieved in a mean state with smaller $\Delta\bar{Z}500$ (see Figure 4 in *Screen and Simmonds* [2013] for an illustration). However, this argument overlooks the fact that the strength of the anomalies also changes with ΔT_y. As demonstrated in Figure 2 and discussed in section 3.2, the strength of the anomalies increases (almost proportionally to $\Delta\bar{Z}500$) as ΔT_y rises. The proportional change in this simple analysis suggests that the wave amplitude should remain the same; hence, explaining the positive trends in Figure 4 requires accounting for other processes and further investigation.

4. Conclusions

Francis and Vavrus [2012] and *Liu et al.* [2012] (FVL12) have recently proposed a dynamical link between midlatitude weather extremes and changes in the Arctic. They argue that a smaller midlatitude to pole, near-surface temperature difference ΔT, due to Arctic Amplification (AA), leads to slower zonal winds and decreases the midlatitude meridional gradient of $Z500$ ($\Delta\bar{Z}500$), resulting in more blocks and wavier jet streams. Here we study the last part of this argument by investigating more closely the idea that slower

zonal winds and smaller $\Delta\bar{Z}500$ (as a result of reduced ΔT) lead to more blocks and wavier jet streams. To isolate the role of ΔT and obtain clear responses, we use an idealized model, which still retains the physics essential to the proposed mechanism. Our results show a robust decline in blocked area and meridional wave amplitude with reducing ΔT, despite the decrease in zonal winds and $\Delta\bar{Z}500$. Left for future work is identifying the mechanisms that produce these responses and separating their contributions, which can also improve the understanding of blocking dynamics. Although the methods used here to calculate blocking and wave amplitude statistics have been carefully designed and tested, further examination of the sensitivity of the reported statistics is warranted; as such, statistics can be sensitive to methodology [*Barnes*, 2013; *Screen and Simmonds*, 2013; *Barnes et al.*, 2014].

This work focuses only on the hypothesis of FVL12, and while our idealized setup employs various simplifications and lacks some physical processes, the excluded processes are not essential to the proposed mechanism. Furthermore, the response of the model's mean state to AA-like forcings is fairly consistent with observations, although there are uncertainties regarding the direction of the jet latitude shift. Whether the presence of forced quasi-stationary planetary waves changes the response of blocks and (particularly) wave amplitude to ΔT remains an open question requiring further investigation. With the limitations of an idealized approach in mind, we suggest that our findings provide a complement to the current studies with a hierarchy of GCMs and observation to examine and understand the mechanism of FVL12. We further emphasize that the influences of AA on midlatitude blocking and wave amplitude through mechanisms other than the one discussed above is beyond the scope of this study.

Acknowledgments

The authors thank Edwin Gerber, Isaac Held, Peter Huybers, Phil Marcus, Ji Nie, and Andy Rhines for fruitful discussions; Ding Ma, Mary Moore, and Andy Rhines for helpful comments on the manuscript; and Chris Walker for generous help with GCM runs. The authors are grateful to Jennifer Francis and an anonymous reviewer for insightful comments and suggestions which greatly improved the manuscript. This research was supported by a Ziff Environmental Fellowship from Harvard University Center for the Environment (PH) and NSF grants AGS-0754332 and AGS-1062016 (ZK), and AGS-1246929 (BFF). The simulations were run on Harvard Odyssey cluster. The data for this paper are available upon request.

The Editor thanks Jennifer Francis and an anonymous reviewer for their assistance in evaluating this paper.

References

Anstey, J. A., P. Davini, L. J. Gray, T. J. Woollings, N. Butchart, C. Cagnazzo, and S. Yang (2013), Multi-model analysis of Northern Hemisphere winter blocking: Model biases and the role of resolution, *J. Geophys. Res. Atmos.*, *118*, 3956–3971, doi:10.1002/jgrd.50231.

Archer, C. L., and K. Caldeira (2008), Historical trends in the jet streams, *Geophys. Res. Lett.*, *35*, L08803, doi:10.1029/2008GL033614.

Barnes, E. A. (2013), Revisiting the evidence linking Arctic amplification to extreme weather in midlatitudes, *Geophys. Res. Lett.*, *40*(17), 4734–4739, doi:10.1002/grl.50880.

Barnes, E. A., and D. L. Hartmann (2010), Influence of eddy-driven jet latitude on North Atlantic jet persistence and blocking frequency in CMIP3 integrations, *Geophys. Res. Lett.*, *37*, L23802, doi:10.1029/2010GL045700.

Barnes, E. A., and L. Polvani (2013), Response of the midlatitude jets, and of their variability, to increased greenhouse gases in the CMIP5 models, *J. Clim.*, *26*(18), 7117–7135, doi:10.1175/JCLI-D-12-00536.1.

Barnes, E. A., J. Slingo, and T. Woollings (2011), A methodology for the comparison of blocking climatologies across indices, models and climate scenarios, *Clim. Dyn.*, *38*(11-12), 2467–2481, doi:10.1007/s00382-011-1243-6.

Barnes, E. A., L. M. Polvani, and A. H. Sobel (2013), Model projections of atmospheric steering of Sandy-like superstorms, *Proc. Natl. Acad. Sci. U. S. A.*, *110*(38), 15,211–15,215, doi:10.1073/pnas.1308732110.

Barnes, E. A., E. Dunn-Sigouin, G. Masato, and T. Woollings (2014), Exploring recent trends in Northern Hemisphere blocking, *Geophys. Res. Lett.*, *41*, 638–644, doi:10.1002/2013GL058745.

Barriopedro, D., R. García-Herrera, A. R. Lupo, and E. Hernández (2006), A climatology of Northern Hemisphere blocking, *J. Clim.*, *19*(6), 1042–1063, doi:10.1175/JCLI3678.1.

Barriopedro, D., R. García-Herrera, and R. M. Trigo (2010), Application of blocking diagnosis methods to general circulation models. Part I: A novel detection scheme, *Clim. Dyn.*, *35*(7–8), 1373–1391, doi:10.1007/s00382-010-0767-5.

Berrisford, P., B. J. Hoskins, and E. Tyrlis (2007), Blocking and Rossby wave breaking on the dynamical tropopause in the Southern Hemisphere, *J. Atmos. Sci.*, *64*(8), 2881–2898, doi:10.1175/JAS3984.1.

Black, E., M. Blackburn, G. Harrison, B. Hoskins, and J. Methven (2004), Factors contributing to the summer 2003 European heatwave, *Weather*, *59*(8), 217–223, doi:10.1256/wea.74.04.

Buehler, T., C. C. Raible, and T. F. Stocker (2011), The relationship of winter season North Atlantic blocking frequencies to extreme cold or dry spells in the ERA-40, *Tellus A*, *63*(2), 212–222, doi:10.1111/j.1600-0870.2010.00492.x.

Butler, A. H., D. W. Thompson, and R. Heikes (2010), The steady-state atmospheric circulation response to climate change-like thermal forcings in a simple general circulation model, *J. Clim.*, *23*(13), 3474–3496, doi:10.1175/2010JCLI3228.1.

Cheung, H. N., H. Y. Mok, M. C. Wu, and Y. Shao (2013), Revisiting the climatology of atmospheric blocking in the Northern Hemisphere, *Adv. Atmos. Sci.*, *30*(2), 397–410, doi:10.1007/s00376-012-2006-y.

Coumou, D., and S. Rahmstorf (2012), A decade of weather extremes, *Nat. Clim. Change*, *2*, 491–496, doi:10.1038/nclimate1452.

D'Andrea, F., et al. (1998), Northern Hemisphere atmospheric blocking as simulated by 15 atmospheric general circulation models in the period 1979–1988, *Clim. Dyn.*, *14*(6), 385–407, doi:10.1007/s003820050230.

Dole, R. M., and N. D. Gordon (1983), Persistent anomalies of the extratropical Northern Hemisphere wintertime circulation: Geographical distribution and regional persistence characteristics, *Mon. Weather Rev.*, *111*(8), 1567–1586.

Dole, R., M. Hoerling, J. Perlwitz, J. Eischeid, P. Pegion, T. Zhang, and D. Murray (2011), Was there a basis for anticipating the 2010 Russian heat wave?, *Geophys. Res. Lett.*, *38*, L06702, doi:10.1029/2010GL046582.

Dunn-Sigouin, E., and S. W. Son (2013), Northern Hemisphere blocking frequency and duration in the CMIP5 models, *J. Geophys. Res. Atmos.*, *118*, 1179–1188, doi:10.1002/jgrd.50143.

Francis, J. A., and S. J. Vavrus (2012), Evidence linking Arctic amplification to extreme weather in mid-latitudes, *Geophys. Res. Lett.*, *39*, L06801, doi:10.1029/2012GL051000.

Gerber, E. P., and G. K. Vallis (2007), Eddy–zonal flow interactions and the persistence of the zonal index, *J. Atmos. Sci.*, *64*(9), 3296–3311, doi:10.1175/JAS4006.1.
Gerber, E. P., S. Voronin, and L. M. Polvani (2008), Testing the annular mode autocorrelation time scale in simple atmospheric general circulation models, *Mon. Weather Rev.*, *136*(4), 1523–1536, doi:10.1175/2007MWR2211.1.
Green, J. S. A. (1977), The weather during July 1976: Some dynamical considerations of the drought, *Weather*, *32*(4), 120–126.
Held, I. M., and M. J. Suarez (1994), A proposal for the intercomparison of the dynamical cores of atmospheric general circulation models, *Bull. Am. Meteorol. Soc.*, *75*(10), 1825–1830.
Hoerling, M. P., P. A. Stott, and S. C. Herring (2013), Explaining extreme events of 2012 from a climate perspective, *Bull. Am. Meteorol. Soc.*, *94*, S1–S74, doi:10.1175/BAMS-D-13-00085.1.
Hong, C.-C., H.-H. Hsu, N.-H. Lin, and H. Chiu (2011), Roles of European blocking and tropical-extratropical interaction in the 2010 Pakistan flooding, *Geophys. Res. Lett.*, *38*, L13806, doi:10.1029/2011GL047583.
Hu, Y., D. Yang, and J. Yang (2008), Blocking systems over an aqua planet, *Geophys. Res. Lett.*, *35*, L19818, doi:10.1029/2008GL035351.
Intergovernmental Panel on Climate Change (2007), *Climate Change 2007: The Physical Science Basis. Contribution of Working Group I to the Fourth Assessment Report of the Intergovernmental Panel on Climate Change*, edited by S. Solomon et al., 996 pp., Cambridge Univ. Press, New York.
Kidston, J., and G. K. Vallis (2010), Relationship between eddy-driven jet latitude and width, *Geophys. Res. Lett.*, *37*, L21809, doi:10.1029/2010GL044849.
Kidston, J., and G. K. Vallis (2012), The relationship between the speed and the latitude of an eddy-driven jet in a stirred barotropic model, *J. Atmos. Sci.*, *69*(11), 3251–3263, doi:10.1175/JAS-D-11-0300.1.
Kunz, T., K. Fraedrich, and F. Lunkeit (2009), Synoptic scale wave breaking and its potential to drive NAO-like circulation dipoles: A simplified GCM approach, *Q. J. R. Meteorol. Soc.*, *135*(638), 1–19, doi:10.1002/qj.351.
Liu, J., J. A. Curry, H. Wang, M. Song, and R. M. Horton (2012), Impact of declining Arctic sea ice on winter snowfall, *Proc. Natl. Acad. Sci. U. S. A.*, *109*(11), 4074–4079, doi:10.1073/pnas.1114910109.
Liu, Z., K. Yoshimura, G. J. Bowen, N. H. Buenning, C. Risi, J. M. Welker, and F. Yuan (2014), Paired oxygen isotope records reveal modern North American atmospheric dynamics during the Holocene, *Nat. Commun.*, *5*(3701), doi:10.1038/ncomms4701.
Lu, J., G. Chen, and D. M. Frierson (2008), Response of the zonal mean atmospheric circulation to El Niño versus global warming, *J. Clim.*, *21*(22), 5835–5851, doi:10.1175/2008JCLI2200.1.
Lu, J., G. Chen, and D. M. W. Frierson (2010), The position of the midlatitude storm track and eddy-driven westerlies in aquaplanet AGCMs, *J. Atmos. Sci.*, *67*(12), 3984–4000, doi:10.1175/2010JAS3477.1.
Nakamura, H., M. Nakamura, and J. L. Anderson (1997), The role of high- and low-frequency dynamics in blocking formation, *Mon. Weather Rev.*, *125*(9), 2074–2093.
Park, T.-W., C.-H. Ho, and S. Yang (2011), Relationship between the Arctic Oscillation and cold surges over East Asia, *J. Clim.*, *24*(1), 68–83, doi:10.1175/2010JCLI3529.1.
Peings, Y., and G. Magnusdottir (2014), Response of the wintertime Northern Hemisphere atmospheric circulation to current and projected Arctic sea ice decline: A numerical study with CAM5, *J. Clim.*, *27*(1), 244–264, doi:10.1175/JCLI-D-13-00272.1.
Pelly, J. L., and B. J. Hoskins (2003), A new perspective on blocking, *J. Atmos. Sci.*, *60* (5), 743–755, doi:10.1175/1520-0469(2003)060<0743:ANPOB>2.0.CO;2.
Polvani, L. M., and P. J. Kushner (2002), Tropospheric response to stratospheric perturbations in a relatively simple general circulation model, *Geophys. Res. Lett.*, *29*(7), 1114, doi:10.1029/2001GL014284.
Rex, D. F. (1950), Blocking action in the middle troposphere and its effect upon regional climate, *Tellus*, *2*(3), 196–211.
Rinke, A., K. Dethloff, W. Dorn, D. Handorf, and J. C. Moore (2013), Simulated Arctic atmospheric feedbacks associated with late summer sea ice anomalies, *J. Geophys. Res. Atmos.*, *118*(14), 7698–7714, doi:10.1002/jgrd.50584.
Riviére, G. (2011), A dynamical interpretation of the poleward shift of the jet streams in global warming scenarios, *J. Atmos. Sci.*, *68*(6), 1253–1272, doi:10.1175/2011JAS3641.1.
Sausen, R., W. König, and F. Sielmann (1995), Analysis of blocking events from observations and ECHAM model simulations, *Tellus A*, *47*(4), 421–438.
Screen, J. A. (2014), Arctic amplification decreases temperature variance in northern mid- to high-latitudes, *Nat. Clim. Change*, *4*, 577–582, doi:10.1038/nclimate2268.
Screen, J. A., and I. Simmonds (2010), The central role of diminishing sea ice in recent Arctic temperature amplification, *Nature*, *464*, 1334–1337, doi:10.1038/nature09051.
Screen, J. A., and I. Simmonds (2013), Exploring links between Arctic amplification and mid-latitude weather, *Geophys. Res. Lett.*, *40*(5), 959–964, doi:10.1002/grl.50174.
Screen, J. A., and I. Simmonds (2014), Amplified mid-latitude planetary waves favour particular regional weather extremes, *Nat. Clim. Change*, doi:10.1038/nclimate2271.
Screen, J. A., C. Deser, I. Simmonds, and R. Tomas (2013), Atmospheric impacts of Arctic sea-ice loss, 1979–2009: Separating forced change from atmospheric internal variability, *Clim. Dyn.*, 1–12, doi:10.1007/s00382-013-1830-9.
Shabbar, A., J. Huang, and K. Higuchi (2001), The relationship between the wintertime North Atlantic Oscillation and blocking episodes in the North Atlantic, *Int. J. Climatol.*, *21*(3), 355–369, doi:10.1002/joc.612.
Shukla, J., and K. C. Mo (1983), Seasonal and geographical variation of blocking, *Mon. Weather Rev.*, *111*(2), 388–402.
Tang, Q., X. Zhang, and J. A. Francis (2013a), Extreme summer weather in northern mid-latitudes linked to a vanishing cryosphere, *Nat. Clim. Change*, *4*, 45–50, doi:10.1038/nclimate2065.
Tang, Q., X. Zhang, X. Yang, and J. A. Francis (2013b), Cold winter extremes in northern continents linked to Arctic sea ice loss, *Environ. Res. Lett.*, *014,036*(1), doi:10.1088/1748-9326/8/1/014036.
Trigo, R. M., I. F. Trigo, C. C. DaCamara, and T. J. Osborn (2004), Climate impact of the European winter blocking episodes from the NCEP/NCAR Reanalyses, *Clim. Dyn.*, *23*(1), 17–28, doi:10.1007/s00382-004-0410-4.
Tyrlis, E., and B. J. Hoskins (2008), Aspects of a Northern Hemisphere atmospheric blocking climatology, *J. Atmos. Sci.*, *65*(5), 1638–1652, doi:10.1175/2007JAS2337.1.
Vihma, T. (2014), Effects of Arctic sea ice decline on weather and climate: A review, *Surv. Geophys.*, 1–40, doi:10.1007/s10712-014-9284-0.
Walker, C. C., and T. Schneider (2006), Eddy influences on Hadley circulations: Simulations with an idealized GCM, *J. Atmos. Sci.*, *63*(12), 3333–3350, doi:10.1175/JAS3821.1.

Wallace, J. M., I. M. Held, D. W. Thompson, K. E. Trenberth, and J. E. Walsh (2014), Global warming and winter weather, *Science*, *343*(6172), 729–730.

Walsh, J. E. (2014), Intensified warming of the Arctic: Causes and impacts on middle latitudes, *Global Planet. Change*, *117*, 52–63, doi:10.1016/j.gloplacha.2014.03.003.

Woollings, T. J., B. J. Hoskins, M. Blackburn, and P. Berrisford (2008), A new Rossby wave–breaking interpretation of the North Atlantic Oscillation, *J. Atmos. Sci.*, *65*(2), 609–626, doi:10.1175/2007JAS2347.1.

Woollings, T., B. Harvey, and G. Masato (2014), Arctic warming, atmospheric blocking and cold European winters in CMIP5 models, *Environ. Res. Lett.*, *014,002*(1), doi:10.1088/1748-9326/9/1/014002.